

# Enhanced Active Disturbance Rejection Current Controller for Permanent Magnet Synchronous Machines Operated at Low Sampling Time Ratio

Ahmed M. Diab, *Graduate Student Member, IEEE*, Seang Shen Yeoh, Serhiy Bozhko, *Senior Member, IEEE*, Chris Gerada, *Senior Member, IEEE* and Michael Galea, *Senior Member, IEEE*

**Abstract**—Recently, Active Disturbance Rejection Control (ADRC) Scheme has been widely used for current regulation in AC drive systems owing to its robustness to system uncertainties and its high disturbance-rejection capability. However, it has not been considered as an option for high-speed drives usually operated at limited switching and sampling frequencies. Therefore, this paper thoroughly analyses and discusses the effects of high operating speed, modulation, and computational delays on the conventional ADRC. Based on this analysis, an enhanced ADRC for the current control is proposed to operate the drive system at low sampling time ratio with high robustness to the internal and external disturbances. Effect of model uncertainties on the proposed scheme has also been analytically analyzed and reported. Comprehensive simulation and experimental results have been presented to demonstrate the improved performance of the proposed ADRC scheme and to support the analytical studies.

**Index Terms**—Active disturbance rejection control, current controller, permanent Magnet Synchronous Machine, Smith predictor.

## I. INTRODUCTION

HIGH-speed and high-power permanent magnet synchronous machines (PMSMs) have seen a rapid growth of use in last few decades due to their high-power density and reliability. They have been adopted in many considerable applications such as starter/generator, actuation systems and electric vehicles [1]. For these applications, both dynamic and steady state performances provided by the control are crucial [2, 3]. This can be a challenge, as operating the machine at high speeds may lead to unstable operation owing to a relatively low sampling to fundamental frequency ratio (low sampling time ratio (LST)) [4, 5]. Operating the machines at high speeds with limited switching and sampling frequencies affects the performance of the machine control loop as fewer

measurement points are available for reliable current tracking. As such, there is considerable research effort being made recently, to improve the current control dynamics of PMSMs at LST ratio which are normally lower than 15 [4, 6]. These improvements are basically to provide proper compensation for the cross-coupling terms which would degrade the system stability at LST ratio and limit the system bandwidth at high operating speed [7].

The most popular current controller scheme that has plenty of development in this field is the synchronous reference frame (SRF) proportional integral (PI) current controller (CC). The enhancement of this controller's performance is done by introducing the cross-coupling components as feedforward terms to achieve a decoupling effect to enhance its dynamic performance [8, 9]. The complex vector structure of SRF PI CC has been proposed to provide better cross coupling compensation and less dependency on the machine parameters [10]. Moreover, direct design of complex SRF PI CC in discrete time domain has been addressed in [4, 7] to avoid the degradation of system performance due to digitalization of the continuous domain PI current controllers. However, the complex PI CC structure has low disturbance rejection capability and additional damping element is required [11] which leads to excessive noise and current ripple in current-controlled inverter applications [12]. On the other hand, optimal tuning of the PI gains depends heavily on accurate knowledge of machine parameters. Any errors or uncertainties in these can affect the drive performance. Machine parameters may also significantly vary during the operation from effects such as temperature variation, saturation, cross saturation, and operating frequencies [13, 14]. It is therefore clear that all these internal disturbances in addition to the external disturbances can lead to performance degradations of a PMSM drive.

At present, several methods on parameter estimation and

This paragraph of the first footnote will contain the date on which you submitted your paper for review. It will also contain support information, including sponsor and financial support acknowledgment. For example, "This work was supported in part by the Department of Commerce under Grant BS123456."

Ahmed M. Diab and Michael Galea are with the Key Laboratory of More Electric Aircraft Technology of Zhejiang Province, University of Nottingham Ningbo China, Ningbo 315100, China (e-mail:

ahmed.diab@nottingham.edu.cn ; michael.galea@nottingham.edu.cn) and Powe Electronic and Machine Control Group, University of Nottingham, Nottingham, NG7 2RD, UK (e-mail: ahmed.diab@nottingham.ac.uk ; michael.galea@nottingham.ac.uk).

Serhiy Bozhko, Seang Shen Yeoh and Christopher Gerada are with the Power Electronics, Machines and Control Group, University of Nottingham, Nottingham NG7 2RD, U.K. (e-mail: serhiy.bozhko@nottingham.ac.uk ; chris.gerada@nottingham.ac.uk ; seang.yeoh@nottingham.ac.uk)

disturbance rejection are reported. State observers (SO) and disturbance observers (DOB) have a long history of being used to overcome the effects of external disturbances [15-17]. These observers have been identified as the most effective way to estimate the disturbance that lump together model uncertainties and external disturbances. The SO can be extended not only to estimate the external disturbance but also to estimate the internal disturbances which cover the unknown parameters. This “extended state observer” (ESO) proposed in [18] is combined with the active disturbance rejection control (ADRC) concept which has been used in industry as an alternative scheme for the classical PI controller [19, 20].

The superior performance of the ADRC scheme for AC drive current control has been proven in [21]. This is due to simplicity in implementation and higher disturbance rejection capability compare to other control techniques [22]. The design criterion of the ADRC as a current controller has been addressed in [23] but effects of operating speeds which degrade the system stability during the operation has not been discussed. Moreover, in the literature, this scheme has not yet been considered as an option for high-speed machines usually operated at LST ratio. Therefore, the paper firstly analyses and evaluates effects of higher operating speeds with limited sampling points of a PMSM drive system, modulation and digital computational delay on current control system stability and dynamics when the conventional ADRC is used. This is considered a novel analysis that shows the lack of ADRC scheme as a CC and evaluate its limitation to provide higher operating speeds at fixed switching frequency which might be limited in some industrial applications due to the cost and efficiency reasons. Then, an enhanced ADRC scheme is proposed based on Smith predictor (SP) which has been introduced in the literature [24, 25] to mitigate time delay effects on the control system dynamics. It has been implemented in this paper with the conventional ADRC based current controller to improve the system’s robustness to the internal and external disturbances at LST ratio operation. The scheme performance has been analyzed and compared against the conventional one. Effects of model uncertainties have also been analyzed and reported. Comprehensive simulation and experimental testing are reported to validate performance of the proposed active disturbance rejection current controller (ADRCC) scheme and to support the analytical studies of this research.

## II. CONVENTIONAL ADRC SCHEME BASED CURRENT CONTROLLER

The PMSM electrical model can be represented by two voltage equations depicted in  $dq$  synchronous reference frame as follows [20], where  $i_{d,q}$ ,  $v_{d,q}$ ,  $L_{d,q}$  and  $d_{d,q}$ , correspond to  $d,q$  axis stator current, voltages, inductances, and external disturbances, respectively.  $r_s$  is stator resistance, and  $\omega_r$  is electrical angular velocity.  $\phi_m$  is flux linkage of PMSM:

$$\begin{cases} \frac{di_d}{dt} = -\frac{r_s}{L_d} i_d + \omega_r \frac{L_q}{L_d} i_q - \frac{1}{L_d} d_d + \frac{1}{L_d} u_d \\ \frac{di_q}{dt} = -\frac{r_s}{L_q} i_q - \omega_r \frac{L_d}{L_q} i_d - \frac{1}{L_q} \omega_r \phi_m - \frac{1}{L_q} d_q + \frac{1}{L_q} u_q \end{cases} \quad (1)$$

Considering the current control based on ADRC [10], equation (1) can be re-written as (2), where  $f_d$  and  $f_q$  represent the generalized disturbance in  $d$  and  $q$  axes respectively that lump the external disturbances and process dynamics.

$$\begin{cases} \frac{di_d}{dt} = f_d(t, i_d, i_q, d_d, \omega_r) + \frac{1}{L_d} u_d \\ \frac{di_q}{dt} = f_q(t, i_d, i_q, d_q, \omega_r, \phi_m) + \frac{1}{L_q} u_q \end{cases} \quad (2)$$

As follows from (2), description of the voltage equations in both  $d$  and  $q$  axes based on ADRC principle is similar. Therefore, the CC structure based on ADRC is symmetrical in  $d$  and  $q$  axes. Since the generalized disturbances  $f$  in  $d$ - or  $q$ -axis are unavailable in practice, an ESO can be built for their estimation in real time under assumption that  $f$  is differentiable with respect to  $t$  and its differential is bounded. The ESO-based feedback control is then used to compensate the generalized disturbance. The block diagram of the current control loop based on ADRC principle in  $q$ -axis is shown in Fig. 1. It is seen that the original system (machine model) can be considered as one integrator with the generalized disturbance  $f_q$  acting on its input. Both ESO and state feedback controller as components of the CC based on ADRC scheme, are discussed below considering the current control loop in the  $q$ -axis.

### A. Extended state observer design

The ESO of  $q$ -axis current controller is designed based on the second order state space model given by (3), which is derived from (1) where  $u_o(t) = u_q(t)$ ,  $b_o = 1/L_q$  and representing the  $q$ -axis by 2 states  $x_q(t) = [x_1(t) \ x_2(t)]^T$ .  $x_1(t)$  is machine current component in the  $q$ -axis and  $x_2(t)$  is the generalized disturbance  $f_q$ . Note that  $[\cdot]^T$  is denoted as the matrix transpose.

$$\begin{cases} \dot{x}_q(t) = A_q x_q(t) + B_q u_o(t) + E_q \dot{f}_q(t) \\ y(t) = C_q x_q(t) \end{cases} \quad (3)$$

where  $A_q = \begin{bmatrix} 0 & 1 \\ 0 & 0 \end{bmatrix}$ ,  $B_q = \begin{bmatrix} b_o \\ 0 \end{bmatrix}$ ,  $E_q = \begin{bmatrix} 0 \\ 1 \end{bmatrix}$ ,  $C_q = [1 \ 0]$

The corresponding ESO can be designed as given by (4), where the value of  $b_o$  has been replaced by  $b_o' = 1/L_q'$ ,  $L_q'$  is the inductance value used in controller design which might be different than the actual machine inductance,  $l_1$  and  $l_2$  are observer gains,  $z_q$  is the estimated states for  $x_q$ ,  $z_q(t) = [z_1(t) \ z_2(t)]^T$  and  $L_c = [l_1 \ l_2]^T$ .

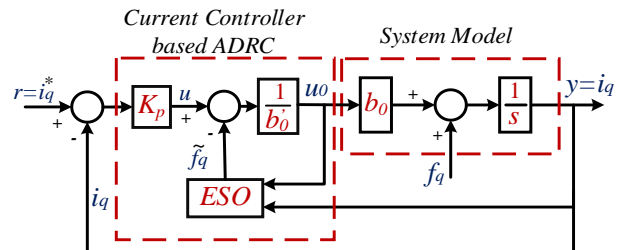


Fig. 1 Current control loop in  $q$ -axis based on the conventional ADRCC scheme

$$\begin{cases} \dot{z}_q(t) = [A_q - L_c C_q] z_q(t) + B_q' u_o(t) + L_c y_q(t) \\ \hat{y}(t) = C_q z_q(t) \end{cases} \quad (4)$$

The target of any observer is to achieve fast and accurate convergence between estimated and actual states. Hence, the observer gains are determined based on the desirable dynamics of estimation error (5) which can be derived using (3) and (4) as shown by (6).

$$\dot{e} = \dot{x} - \dot{z} \quad (5)$$

$$\begin{bmatrix} \dot{e}_1 \\ \dot{e}_2 \end{bmatrix} = \underbrace{\begin{bmatrix} -l_1 & 1 \\ -l_2 & 0 \end{bmatrix}}_{\tilde{A}} \begin{bmatrix} e_1 \\ e_2 \end{bmatrix} \quad (6)$$

To tune the observer gains, the pole placement method can be used [26]. This sets the location of the observer poles ( $S_{ESO1}$  and  $S_{ESO2}$ ) as shown by (7):

$$\Delta = |SI - \tilde{A}| = (s - S_{ESO1})(s - S_{ESO2}) = s^2 + l_1 s + l_2 \quad (7)$$

Typically, in a Linear ADRC (LADRC), ESO poles are set to be equal based on the popular bandwidth parametrization method [22]. Consequently, observer gains can then be chosen as shown in (8), where  $\omega_o$  represents the observer bandwidth.

$$\begin{cases} l_1 = 2 \omega_o \\ l_2 = \omega_o^2 \end{cases} \quad (8)$$

### B. State feedback controller

The feedback controller can be designed based on system output and estimated variable (estimated generalized disturbance) from ESO using the control law as expressed by (9) [22], where  $K_p$  is controller gain,  $r$  represents system input which is consider in our case is the reference value of  $q$ -axis current and  $u$  is the control signal generated from the feedback controller [27].

$$u(t) = K_p(r(t) - y(t)) \quad (9)$$

From Fig. 1, equation (9) can be expressed as (10), considering ability of the disturbance rejection, where  $u_o$  is CC output.

$$u_o(t) = \frac{1}{b'_o} (K_p(r(t) - y(t)) - \tilde{f}_q) \quad (10)$$

It can be observed from CC structure based on ADRC that the cross-coupling terms are considered as a part of the generalized disturbance which should be estimated by ESO. Accordingly, the estimated disturbance is responsible for the cross-coupling compensation. On the other hand, it is well known that the imperfect cross-coupling compensation affects system dynamics when the operating speed increases and might lead to instability as the sampling time ratio reduces [28].

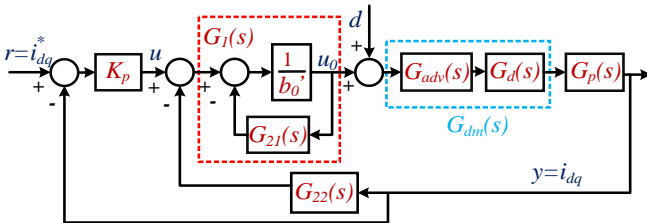


Fig.2 Complex vector representation of the current control loop based on conventional ADRC scheme using the simplified ESO model

Therefore, sensitivity of the current control system based on conventional ADRC scheme to the operational frequency has been analyzed in the following section.

### III. OPERATIONAL FREQUENCY EFFECTS ON THE CONVENTIONAL ADRC STABILITY

Current control loop has been modeled and analyzed in this section considering the ESO dynamics, cross coupling terms, computational and modulation delays. The system model has been derived based on the block diagram shown in Fig. 2. It represents the current control loop based on ADRC scheme for analysis in this section.

In Fig. 2, machine model  $G_p(s)$  has been represented by complex vector representation method (11) which has been derived from (1) based on the complex vector notation [29, 30], where  $L$  refers to machine inductance in  $d$ - or  $q$ -axis.

$$G_p(s) = \frac{i_{dq}^e(s)}{u_{dq}^e(s)} = \frac{1}{Ls + r_s + j\omega_r L} \quad (11)$$

Accordingly, the loop can be analyzed as a single input single output system considering effects of the cross coupling terms, which are represented by  $j\omega_r L$  in the transfer function, which is considered one of the advantages of complex vector representation method [10]. The ESO model has been represented by two separate blocks based on (12) which can be derived from the representation of (4) in s-domain as follows:

$$\begin{bmatrix} Z_1(s) \\ Z_2(s) \end{bmatrix} = \begin{bmatrix} G_{11} & G_{12} \\ G_{21} & G_{22} \end{bmatrix} \begin{bmatrix} U_o(s) \\ Y(s) \end{bmatrix} \quad (12)$$

$$\text{where } G_{11} = \frac{b'_o s}{s^2 + l_1 s + l_2}, \quad G_{12} = \frac{l_1 s + l_2}{s^2 + l_1 s + l_2}$$

$$G_{21} = \frac{-b'_o l_2}{s^2 + l_1 s + l_2}, \quad G_{22} = \frac{l_2 s}{s^2 + l_1 s + l_2}$$

The delay in controller (discrete-time implementation using DSP) and inverter is represented by  $G_d(s)$ . It is modelled in  $dq$  synchronous reference frame as shown by (13), where  $T_d$  is the time delay and it is assumed to be 1.5 the sampling time period [2].

$$G_d(s) = e^{-s T_d} e^{-j\omega_r T_d} \quad (13)$$

To mitigate the delay effect on system performance, advanced angle delay  $G_{adv}$  is taken in consideration which is modelled by (14) [8]. Consequently, resultant system delay in Fig. 2 can be represented in stationary reference frame by (15) which can be approximated with good accuracy by second order pade expansion [2]. The input signal  $d$  in Fig. 2 refers to the external disturbances.

$$G_{adv} = e^{j\omega_e T_d} \quad (14)$$

$$G_{dm}(s) = e^{-s T_d} \cong \frac{1 - \frac{T_d}{2} s + \frac{T_d^2}{12} s^2}{1 + \frac{T_d}{2} s + \frac{T_d^2}{12} s^2} \quad (15)$$

Based on Fig. 2, open and closed loop transfer functions of current control system based on ADRC scheme can be derived

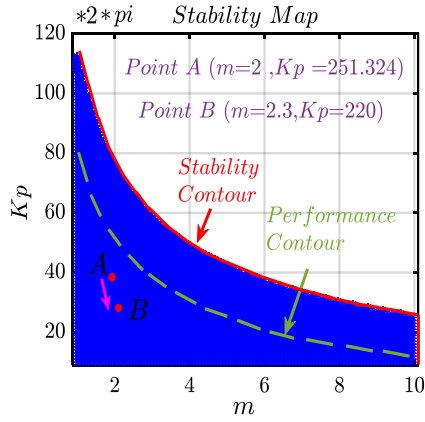


Fig. 3 Stability map for the current controller gains at  $f_{sw}=1$  kHz

as shown in (16) and (17) respectively, where coefficients of (17) are shown in Appendix.

$$G_{o,l1}(s) = K_p \frac{G_1 G_p G_{dm}}{1 + G_1 G_p G_{dm} G_{22}} \quad (16)$$

$$G_{c,l1}(s) = \frac{(s^2 + l_1 s + l_2)(y_2 s^2 + y_1 s + y_0)}{t_5 s^5 + t_4 s^4 + t_3 s^3 + t_2 s^2 + t_1 s + t_0} \quad (17)$$

Based on the characteristics equation of (17), operating frequency's effect on current control system stability can be studied. The study in this paper assumes controlling PMSM with parameters given in Table I where switching frequency has been set at 1kHz to simulate the LST ratio [4].

Observer and feedback controller gains for this analysis are tuned using the stability map shown in Fig. 3 proposed in [23]. The parameter  $m$  in the map is the ratio between observer bandwidth  $\omega_o$  to feedback controller gain  $K_p$ . The stability map provides a stable range of the controller gains to avoid improper tuning that might lead to low stability margins or even instability. Accordingly, controller gains correspond to point A have been selected ( $K_p=251.324$ ,  $m=2$ ) which located beyond the performance contour to guarantee a responsible dynamic performance for the current control system.

Sensitivity of the current control system to the operating frequency has been studied from the analysis of eigenvalues migration and their stability range (SR) map shown in Fig. 4. SR map shows change of the real part of each pole with the operating frequency that refers to stability margins of the current control loop [31]. It can be observed that all closed-loop poles migrate as the frequency increases where a particular interest is given to the closed loop poles  $p_2$  and  $p_3$ . They migrate towards the imaginary axis of the s-plane which refers to a reduction of system stability margins. These migration of

TABLE I: ELECTRIC DRIVE SYSTEM PARAMETERS

Parameter	SYMBOL	Value
Phase Resistance	$r_s$	1.1Ω
Phase Inductance	$L_d=L_q=L$	7.145mH
Poles pairs	$p$	4
Magnet flux linkage	$\Phi_m$	0.0228 wb
Rated Power	$P_{rated}$	0.75 kw
Switching Frequency	$f_{sw}$	1 kHz
Sampling Frequency	$f_s$	1 kHz
Rated speed	$N_{max}$	2000 rpm
Rated Current	$i_{rated}$	4.6 Amp

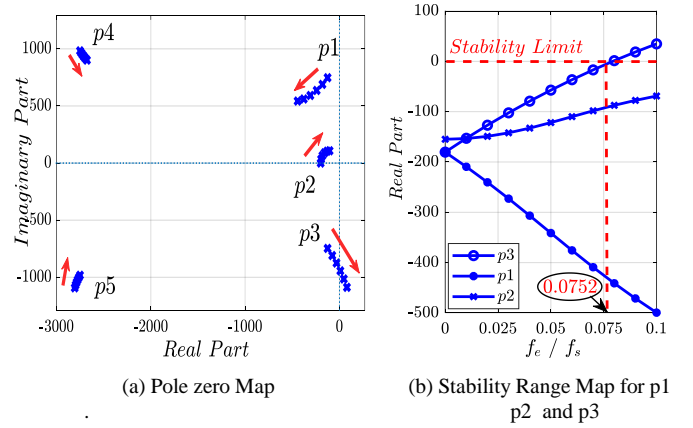


Fig. 4 Migration of the eigenvalues with the operating frequency ( $f_e$ : 0  $\rightarrow$  100 Hz) at  $f_{sw}=1$  kHz,  $m=2$ ,  $K_p=251.324$

eigenvalues shows the lack of the ESO to perfectly compensate the cross-coupling components. As a result, running the machine at higher speeds (at fixed switching frequency) deteriorates system dynamics and leads to instability at certain sampling time ratio. From the (SR) map, it can be observed that the trajectory of  $p_3$  hits the stability limit at about 0.075 as a ratio between the fundamental to the switching frequency. Accordingly, system tends to be unstable at about 14 as a ratio between switching frequency and fundamental frequency. Moreover, this analysis also indicates that the disturbance rejection capability of the ADRC decreases at higher operating speeds due to the lower stability margins. This deterioration of CC's dynamics can be explained by the two following reasons:

1- Estimation Problem: The existence of system delay in the current control system affects ESO performance. Accordingly, it cannot provide accurate estimation for total disturbance. This delay causes misalignment in the time between input and output of the ESO which is clarified by Fig. 5 and explained mathematically from ESO model in (18) [24]. Thus, the ESO is unable to estimate the generalized disturbance accurately.

$$\begin{bmatrix} \frac{di_q}{dt} \\ \tilde{f}_q \end{bmatrix} = \begin{bmatrix} 0 & 1 \\ 0 & 0 \end{bmatrix} \begin{bmatrix} \tilde{i}_q \\ \tilde{x}_2 \end{bmatrix} + \begin{bmatrix} b_o \\ 0 \end{bmatrix} u_{dq} + \begin{bmatrix} l_1 (i_q(t - T_d) - i_q(t)) \\ l_2 (i_q(t - T_d) - i_q(t)) \end{bmatrix} \quad (18)$$

2- Rejection Problem: the cancellation of internal system disturbances by using the ESO cannot be achieved perfectly due to existence of the system delays. This effect enlarges with the operating frequency assuming fixed switching frequency.

To mitigate the aforementioned effects by improving cross-coupling compensation and disturbance rejection capability at

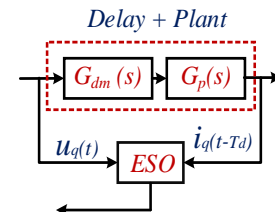


Fig. 5 Delay effect on the ESO inputs

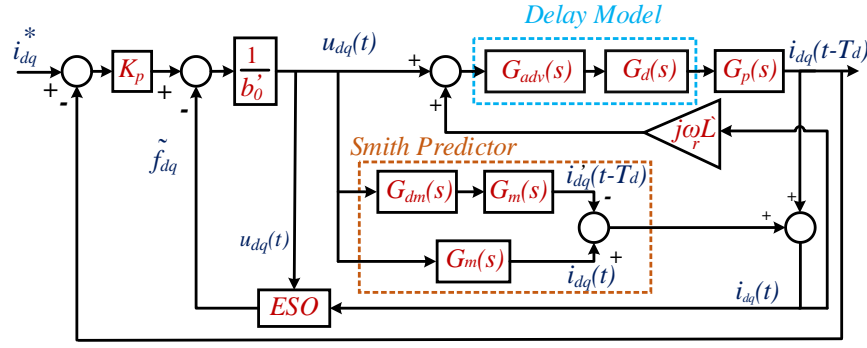


Fig. 6 Block diagram of the current control system based on the proposed ADRCC scheme represented by the complex vector notation

high operating speeds, an enhanced ADRC scheme is proposed in the next Section.

#### IV. ENHANCED ADRC- BASED CURRENT CONTROLLER

The enhanced ADRC scheme is based on SP which can generate prediction current components [24, 25]. These components have been used for two upgrades. First, to enhance ESO dynamics and to provide better estimation for disturbances. So, misalignment between two inputs of the observer due to system delays are removed. Secondly, to generate prediction decoupling current components to enhance the cross-coupling compensation. Subsequently, effects of operating frequency and time delay on the system stability can be reduced. The enhanced ADRCC scheme for current control is shown in Fig. 6. These improvements are discussed and analyzed below.

##### A. Sensitivity to the Operational Frequency

In the enhanced ADRCC scheme given by Fig. 6, SP generates prediction of current components based on the knowledge of system delay  $G_{dm}(s)$  and plant model  $G_m(s)$  that is assumed to match actual plant (machine) model  $G_p(s)$ . Accordingly, output of system model in SP  $i_{dq}'(t-T_d)$  cancels output of actual plant  $i_{dq}(t-T_d)$ . Finally, the output of SP to ESO is  $i_{dq}(t)$  which can be expressed by (19) as a one-step prediction of system output currents.

$$\therefore i_{dq}(t) = \frac{i_{dq}(t-T_d)}{G_{dm}(s)} \quad (19)$$

Accordingly, the block diagram given by Fig. 6 can be simplified in to the one shown in Fig. 7 considering simplified ESO model discussed in Section III. Hence, closed loop transfer function can be derived analytically from Fig. 7 as follows, where coefficients of (22) are shown in the Appendix.

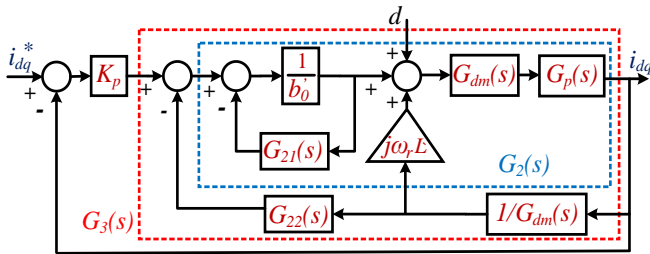


Fig. 7 Complex vector representation of the simplified current control system based on the proposed ADRCC scheme

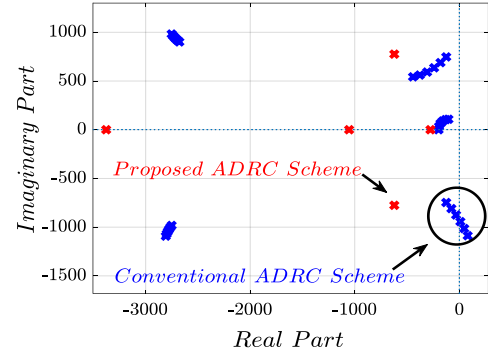


Fig.8 Eigenvalues migration with the conventional (blue) and the proposed (red) ADRCC scheme at  $m=2, K_p=251.324, f_c(0 \rightarrow 100 \text{ Hz})$

$$G_2(s) = \frac{G_{dm}}{(b'_0 + G_{21})(Ls + r_s + j\omega_r(L-L'))} \quad (20)$$

$$G_{ol2}(s) = K_p \frac{G_2 G_{dm}}{G_{dm} + G_2 G_y} \quad (21)$$

$$G_{c.l2}(s) = \frac{i_{dq}}{i_{dqref}} = \frac{X_2(s)}{c_5 s^5 + c_4 s^4 + c_3 s^3 + c_2 s^2 + c_1 s + c_0} \quad (22)$$

The coefficients of characteristic's equation show that there is no dependency on the operating frequency, assuming the errors in machine parameters are neglected. Consequently, system robustness to the operating frequency increases due to complete compensation of the cross-coupling components. As mentioned, the model errors are neglected so that, the robustness issues must be considered. These aspects are analyzed in Section IV.C and verified during experiments.

Based on (22), system eigenvalues are evaluated at different operating frequencies as shown in Fig. 8. One can conclude that the proposed ADRCC scheme enhances system stability and provides high robustness to operating frequency. This refers to its ability to drive the machine at lower sampling time ratio with better stability margins compared to conventional ADRCC scheme.

##### B. Disturbance Rejection Analysis

In this Section, disturbance rejection capability of the proposed scheme is analyzed and compared to the conventional ADRCC. The capability to suppress the disturbance is characterized by output admittance of the current controller [12],  $Y(s) = i_{dq}(s)/d(s)$ , where  $i$  refers to current error due to the

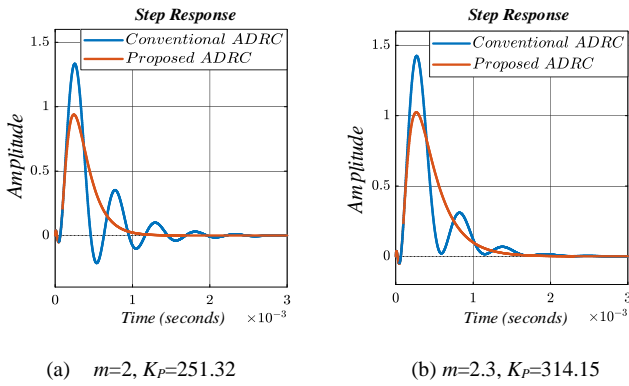


Fig. 9 Step response of the Disturbance rejection transfer functions for the convention and proposed ADRC schemes at different controller settings

disturbances while  $d$  refers to the external disturbance. It is desirable to obtain values of the output admittance as low as possible.

The transfer function between external disturbance  $d$  as an input and the output current has been derived from current control loop considering the proposed scheme shown in Fig.7 as follows:

$$G_{d1}(s) = \frac{i_{dq}}{d} \Big|_{i_{dq}^* = 0} = \frac{G_m(s)G_{dm}(s)}{G_{dm}(s) + K_p G_1(s)G_m(s) + G_{22}(s)G_1(s)G_m(s)} \quad (23)$$

$$\text{where } G_m(s) = \frac{G_{dm}(s)}{L's + r_s'}, \quad G_1(s) = \frac{1}{b'_0 + G_{21}(s)}$$

To analyze the improved disturbance rejection capability using proposed ADRC compared to conventional scheme, disturbance rejection transfer function of the conventional ADRC-based current control loop shown in Fig. 2 is derived as follows:

$$G_{d2}(s) = \frac{i_{dq}}{d} \Big|_{i_{dq}^* = 0} = \frac{G_m(s)}{1 + K_p G_1(s)G_m(s) + G_{22}(s)G_1(s)G_m(s)} \quad (24)$$

Considering the machine parameters in Table I, step response of (23) and (24) has been determined at different controller setting as shown in Fig. 9. It clearly shows that the proposed scheme enhances system stability and provides better disturbance rejection capability to the external disturbances. It can also be noticed that the proposed scheme can enlarge the performance contour in the stability map to cover higher values of controller gains.

Accordingly, high dynamic performance can be achieved at high operating speeds which is considered one of the main challenges for practical design of data-driven fault diagnose and detection schemes [3]. Therefore, it can be stated that the proposed scheme has a potential to be implemented in high-speed applications associated with the fault detections schemes to improve the overall system performance.

### C. Robustness to Model uncertainties

The machine parameters can change during the operation due to temperature and saturation effects. Moreover, the parameters used for controller design typically are not very accurate. These

uncertainties affect system performance, including its stability conditions. Thus, these effects on controller performance have been studied in this section through the analysis of system's eigenvalues migration.

For the changes in machine resistance, migration of current control system eigenvalues is shown in Fig. 10. It is assumed that machine resistance changes from 2 to 0.5 pu. Fig. 10 shows that the eigenvalues do not move significantly which meant that the change of machine resistance has minor effect on enhanced ADRC scheme performance.

For the inductance changes, as it can be observed from Fig.11 that  $p2, p4$  and  $p5$ , for all inductance's sets, are located on real axis having unity damping ratio. Their movement have insignificant impact on CC performance compared to effect of  $p1$  and  $p3$ . At lower machine inductance than its nominal value,  $p1$  and  $p3$  moves toward the imaginary axis which refers to lower damping ratio and stability margins. This refers to a degradation of system stability when the machine inductance decreases. On the other hand, higher machine inductance than the nominal value contributes to  $p1$  and  $p3$  moving towards the real axis away from the imaginary axis which refers to improving system stability and its dynamics.

It can be concluded that the resistance change has insignificant impact on system dynamics compared to the inductance variation. Moreover, the reduction of machine inductance (which happened due to saturation effects)

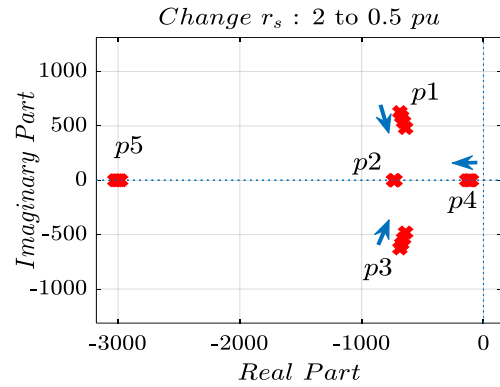


Fig. 10 Migration of the eigenvalues of CC system at different values of machine's resistance

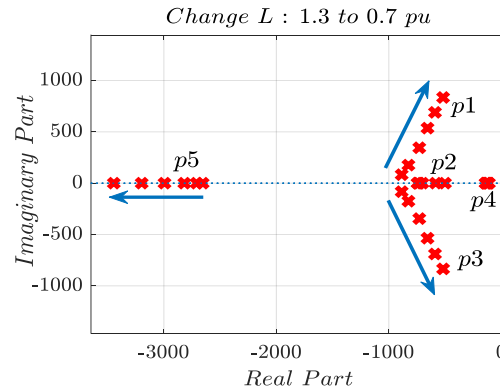


Fig. 11 Migration of the eigenvalues of CC system at different values of machine's inductance

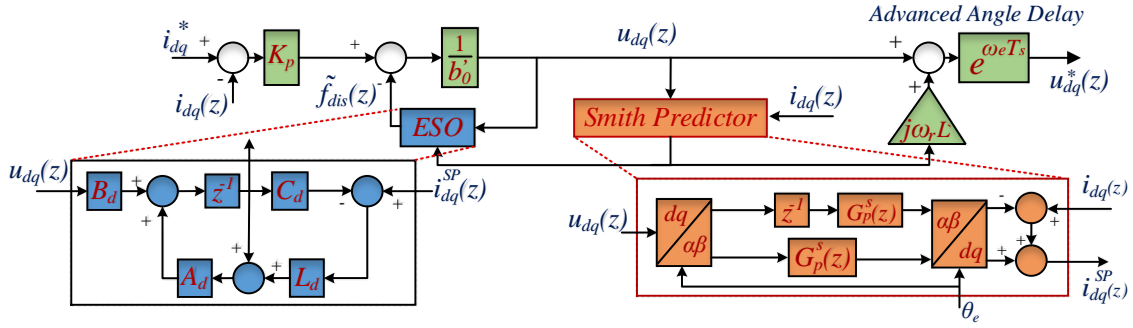


Fig. 12 Block diagram of the proposed ADRCC for digital implementation

deteriorates the system dynamics which can be improved by setting the inductance value used in the controller at lower values (around 0.8 pu for better system robustness to inductance variation).

The digital implementation of the proposed control scheme has been discussed and verified by both time-domain simulations and experiments, as reported in next Sections.

### V. DIGITAL IMPLEMENTATION OF THE PROPOSED ADRC SCHEME

The ESO has been implemented as a current discrete estimator which provides better system stability at low sampling time ratio rather than the predictive discrete estimator as discussed in [32, 33]. Accordingly, ESO mathematical model as a current discrete estimator is shown by (25) which can be derived from (4) using zero order hold approach that maintains same stability properties in both s- and z-domain [32, 34], where  $T_s$  is the sampling time period. Its block diagram for digital implementation can be shown in Fig. 12.

$$\begin{cases} z_q(k+1) = A_d z_q(k) + B_d u_o(k) + A_d L_{dc} y_q(k) \\ \hat{y}_q(k) = C_d z_q(k) \end{cases} \quad (25)$$

$$\text{where } A_d = e^{A_q T_s} = \begin{bmatrix} 1 & T_s \\ 0 & 1 \end{bmatrix}, B_d = \begin{bmatrix} b'_o T_s \\ 0 \end{bmatrix}, C_d = C_q$$

$$L_d = \begin{bmatrix} 1 - \beta^2 \\ (1 - \beta)^2 / T_s \end{bmatrix}, \beta = e^{-\omega_o T_s}$$

As discussed in section III, resultant delay model of current control loop is represented in stationary reference frame by (15). Consequently, SP has been digitally implemented in stationary reference frame as shown in Fig. 12. The discrete model of AC machine in SP is represented in stationary reference frame as follows [4]:

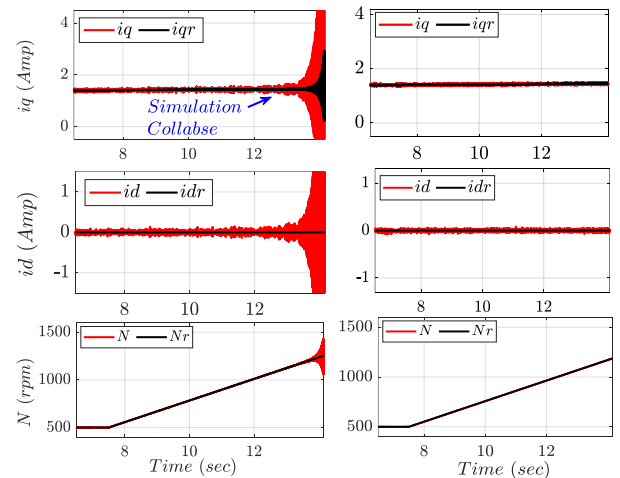
$$G_p^s(z) = \frac{I_{qd}^s(z)}{V_{qd}^s(z)} = \frac{1 - e^{-\frac{r'_s T_s}{L}}}{r'_s (z - e^{-\frac{r'_s T_s}{L}})} \quad (25)$$

As seen from Fig. 12 that the digital implementation of enhanced current controller does not have much difference and complexity than conventional scheme. Only SP and cross-coupling terms are used which are simply added to conventional ADRC scheme during digital implementation. Moreover, no extra gains are required for this upgrade.

### VI. SIMULATION RESULTS

Simulations have been carried out using MATLAB/Simulink in order to test both conventional and proposed ADRCC schemes performance. The CCs have been tested by applying field-oriented control on PMSM drive system (parameters are given in Table I). The CCs are simulated by discrete time blocks as discussed in Section V and the inverter is simulated by its switching model. One step time delay is considered when reference voltage is applied from controller to machine. Sampling frequency has been set equal to switching frequency 1kHz to simulate LST operation.

The gains of observer and feedback controller have been set at same values for both CC schemes (according to Point A in the stability map shown by Fig. 3). In simulation results shown in Fig. 13, the machine reference speed increases gradually from 500 rpm to 1500 rpm ( $f_{sw}/f_e = 30$  to 10) at constant load torque. As shown, conventional ADRC scheme loses the stability at around 1100 rpm ( $f_{sw}/f_e = 13.6$ ) whereas the proposed scheme is able to deliver higher operating speeds by keeping the drive system in stable operation. These results validate the robustness improvement of proposed ADRC to the operational frequency compared to conventional scheme and verify the analytical study in Section III and IV. Hence, the proposed controller is able to drive the machine at much lower sampling time ratio with higher stability margins.



(a) Conventional ADRCC scheme

(b) Proposed ADRCC scheme

Fig. 13 Simulation Results at  $f_{sw}=1$  kHz and speed reference changes from 500 to 1500 rpm,  $K_p=251.32$ ,  $m=2$

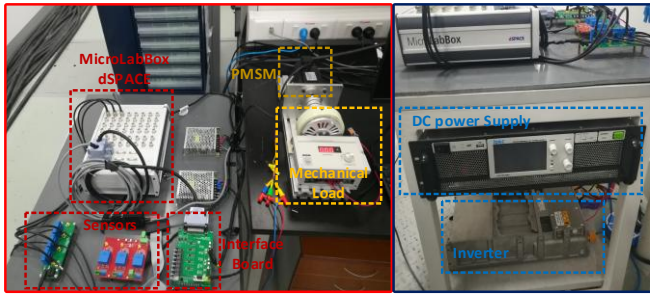


Fig. 14 Experimental test rig

VII. EXPERIMENTAL RESULTS

In order to test conventional and proposed ADRCC schemes at LST ratio, experimental results were carried out using the test rig shown in Fig. 14. The parameters of drive system are same as the simulation. The test rig consists of PMSM with parameters shown in Table I linked to a dynamometer to set a required mechanical loading, and dSPACE MicroLabBox operating as a controller to output the desired PWM signals to the converter.

A. Experimental results at low sampling time ratio

Similar to case study in simulation, the machine reference speed increases gradually from 500 rpm at constant load torque using same controller gains (set to Point A at Fig.3). The experimental results are shown in Fig. 15. The results show the ability of proposed ADRC scheme to deliver higher operating speed compared to conventional ADRC at same switching frequency which validates the derived analytical and simulation results.

It should be mentioned that higher feedback controller gains reduce system stability margins when conventional ADRC is used as explained from Fig. 16. It shows the frequency response of open loop transfer function (16) given in Section III. Accordingly, lower feedback controller gains extend the ability of conventional ADRC as a CC to deliver higher operating

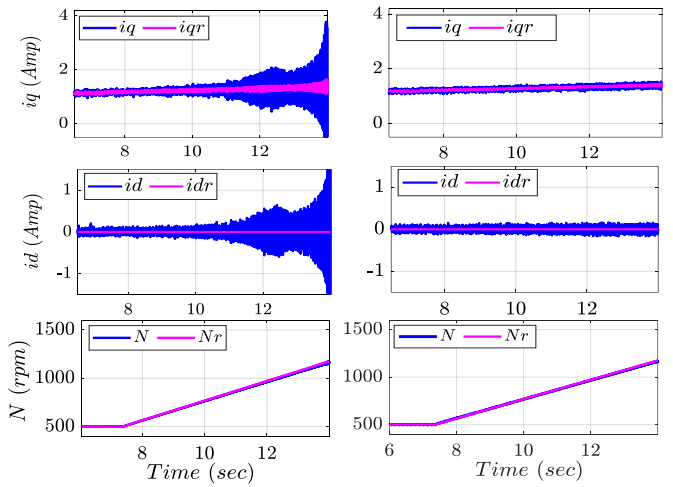


Fig. 15 Experimental Results at  $f_{sw}=1$  kHz and speed reference changes from 500 to 1500 rpm,  $K_p=251.32$ ,  $m=2$

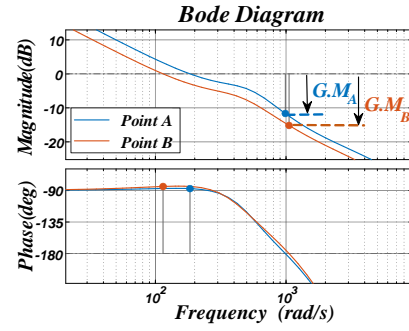


Fig. 16 Frequency response of Equation (16) at two different settings (Point A and Point B)

speeds. Therefore, experiments have been repeated for new gains (set to Point B at Fig.3) where the reference speed increases gradually from 1250 rpm to 1750 rpm ( $f_{sw}/f_e = 12$  to 8.5) as shown in Fig. 17. The results show that the ability of conventional ADRCC to provide lower sampling time ratio is extended as expected from the analytical results. However, it still has a limited operating speed compared to proposed scheme. Moreover, it can be noticed that current waveforms have higher oscillations with conventional ADRC which indicates to lower power quality and stability margins compared to proposed one as seen from Fig.18. It shows the harmonic spectrum analysis for  $i_q$  current components shown in Fig. 17 at 1250 rpm. The results in Fig. 18 show that enhanced ADRCC scheme provides lower current ripple compared to conventional scheme at low switching frequency. Besides, lower feedback controller refers to lower bandwidth which decreases speed of the response.

Load tracking of the proposed ADRCC scheme at LST ratio has also been tested experimentally as reported in Fig. 19. The test has been done by applying different step loads during the operation at 1500 rpm ( $f_{sw}/f_e = 10$ ). The results show that the proposed scheme can provide fast and stable tracking for loads even at low ratio between sampling to operating frequency which verify the outcome of analytical results in Section III and IV-A.

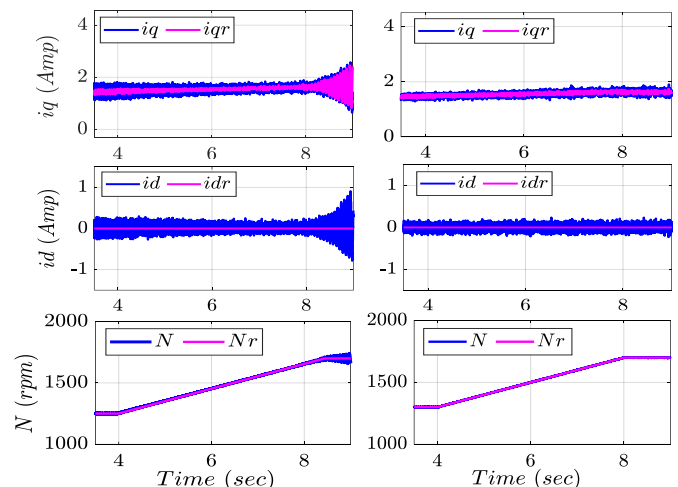


Fig. 17 Experimental Results at  $f_{sw}=1$  kHz and speed reference changes from 1250 to 1750 rpm,  $K_p=220$ ,  $m=2.3$

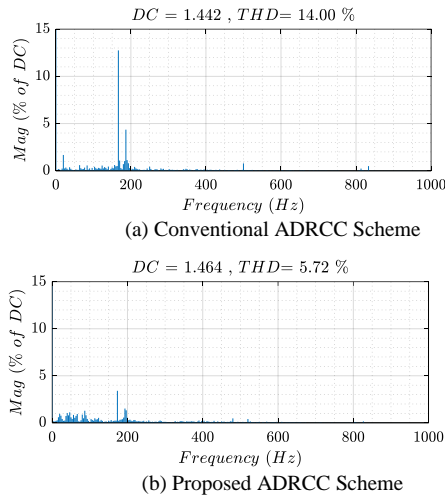


Fig. 18 Harmonic contents of  $i_q$  current at  $f_{sw}/f_c=12$  for conventional and advanced ADRCC schemes

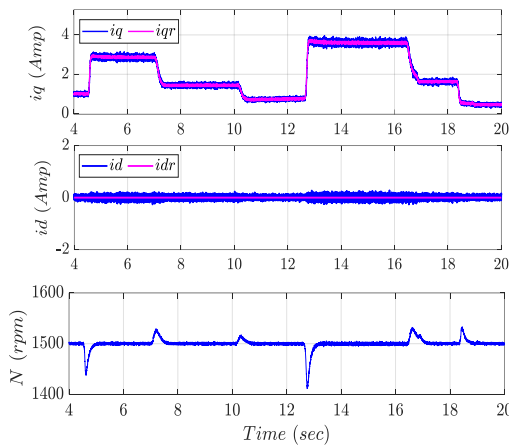


Fig. 19 Experimental Results for step loading at  $f_{sw}/f_c=10$ ,  $K_p=251.32$ ,  $m=2$  for the proposed ADRCC

**B. Disturbance Rejection capability**

The disturbance rejection capability has been tested at 1000 rpm for conventional and proposed ADRCC schemes as shown in Fig. 20. The disturbance is implemented as a step input voltage = 7 v added to reference voltage of the q-axis. The results in Fig. 20 show the ability of proposed CC scheme to provide better rejection for disturbances which verify the analytical study of output admittance in Section IV.B. It can also be observed that the current waveforms are more distorted with the conventional ADRCC than with the enhanced. These results show the ability of proposed CC to enhance power quality of currents waveform and reduce harmonics that can be part of disturbances.

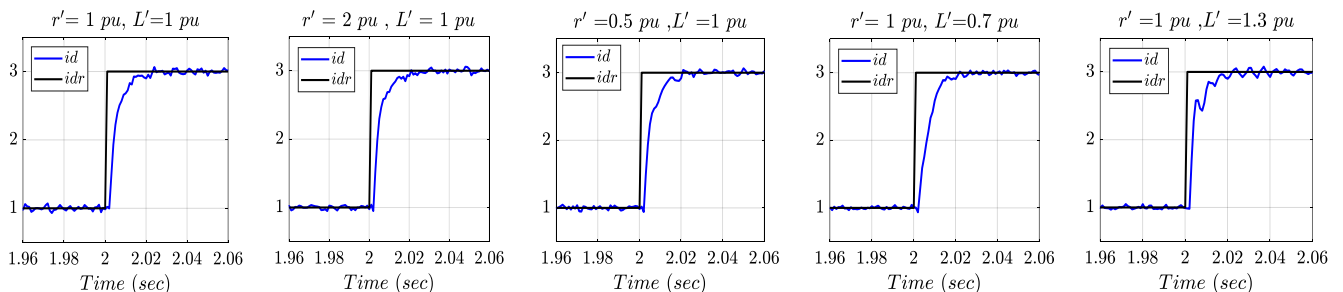


Fig. 21 Experimental results of current response at different values of the machine parameters used in the controller,  $K_p=251.32$ ,  $m=2$

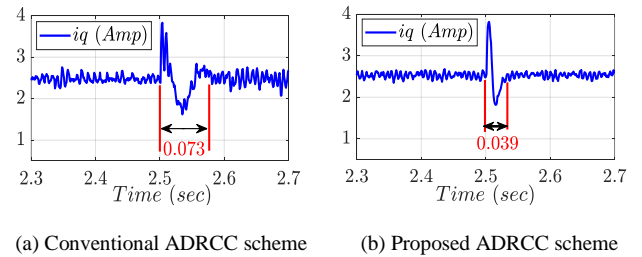


Fig. 20 Experimental results during disturbance for conventional and proposed ADRCC, at 1000 rpm,  $f_{sw}=1$  kHz,  $K_p=220$ ,  $m=2.2$

**C. Robustness to model uncertainties**

The robustness of proposed ADRCC scheme to model uncertainties has been verified experimentally by studying the step response point with locked rotor to provide similar initial conditions for all test cases and to avoid unwanted torque effects. As the decoupled current dynamics for  $d$ - and  $q$ -current are identical, the  $d$ -current reference step response from  $i_d^*=1A$  to  $i_d^*=3A$  has been applied assuming large errors in machine parameters used in controller design. The experimental results are shown in Fig. 21 indicating that the errors in machine resistance value have insignificant effect on the current response. Whereas, for the inductance, it is seen that the system dynamics are deteriorated when higher value of inductance than actual one is used. In opposite, when inductance value is set to be lower than actual value, the system becomes more damped.

Effect of model uncertainties on system dynamics has also been tested through measurement of system response during the disturbance at LST ratio as shown in Fig. 22. Results show that the errors in the predicted machine resistance have insignificant effect on system dynamics. For errors in machine inductance, it can be observed that the system dynamics is more damped and stable when the inductance values used in the controller setting is lower than its nominal value. Whereas the system has lower stability margins at higher inductance values. Accordingly, it can be deduced that setting the inductance value in controller to be lower than the nominal value improves system robustness to reduction of the machine inductance which happened due to saturation effects. These results validate the analytical studies of eigenvalues migration in Section IV.C.

**VIII. CONCLUSION**

In this paper, effect of operating frequency on performance of the current control loop based on ADRC has been analyzed and tested. It has been concluded that the current controller based on conventional ADRC scheme cannot provide

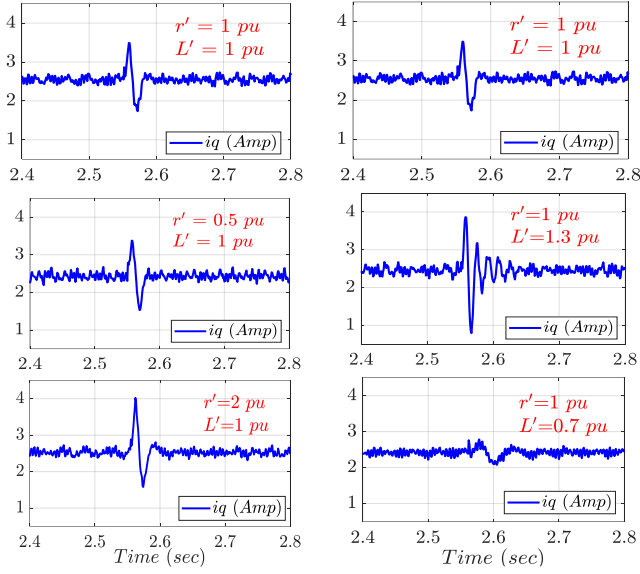


Fig. 22 Experimental results of current response during disturbance for the proposed ADRCC for  $f_{sw}/f_e=10$  at different conditions,  $K_p=251.32$ ,  $m=2$

satisfactory compensation for cross-coupling terms which deteriorates system dynamics at high operating frequency. Accordingly, system loses its stability at certain speed when the sampling time ratio reduces. Moreover, higher operating speeds affects the ESO dynamics hence disturbance rejection capability reduces. An enhanced ADRCC scheme is proposed based on Smith Predictor that predicts the current components. These components improve the observation accuracy of the ESO as they eliminate the misalignment of ESO's inputs. They also generate a prediction decoupling for cross-coupling components. Consequently, the resultant CC scheme is capable of operating the drive system at low sampling time ratio (higher robustness to the operating speed) with high capability to reject internal and externally time-varying disturbances (such as the unpredictable winds and noises). The proposed controller has been analytically studied considering the model uncertainties and the results of this study have been successfully confirmed by detailed time-domain simulations and experiments.

## REFERENCES

- [1] D. Gerada, A. Mebarki, N. L. Brown, C. Gerada, A. Cavagnino, and A. Boglietti, "High-Speed Electrical Machines: Technologies, Trends, and Developments," *IEEE Transactions on Industrial Electronics*, vol. 61, no. 6, pp. 2946-2959, 2014.
- [2] A. G. Yepes, A. Vidal, J. Malvar, O. López, and J. Doval-Gandoy, "Tuning Method Aimed at Optimized Settling Time and Overshoot for Synchronous Proportional-Integral Current Control in Electric Machines," *IEEE Transactions on Power Electronics*, vol. 29, no. 6, pp. 3041-3054, 2014.
- [3] H. Chen, B. Jiang, S. X. Ding, and B. Huang, "Data-Driven Fault Diagnosis for Traction Systems in High-Speed Trains: A Survey, Challenges, and Perspectives," *IEEE Transactions on Intelligent Transportation Systems*, pp. 1-17, 2020.
- [4] H. Kim, M. W. Degner, J. M. Guerrero, F. Briz, and R. D. Lorenz, "Discrete-Time Current Regulator Design for AC Machine Drives," *IEEE Transactions on Industry Applications*, vol. 46, no. 4, pp. 1425-1435, 2010.
- [5] S. Walz, R. Lazar, G. Buticchi, and M. Liserre, "Dahlin-Based Fast and Robust Current Control of a PMSM in Case of Low Carrier Ratio," *IEEE Access*, vol. 7, pp. 102199-102208, 2019.
- [6] M. Hinkkanen, H. A. A. Awan, Z. Qu, T. Tuovinen, and F. Briz, "Current Control for Synchronous Motor Drives: Direct Discrete-Time Pole-Placement Design," *IEEE Transactions on Industry Applications*, vol. 52, no. 2, pp. 1530-1541, 2016.
- [7] N. Hoffmann, F. W. Fuchs, M. P. Kazmierkowski, and D. Schröder, "Digital current control in a rotating reference frame - Part I: System modeling and the discrete time-domain current controller with improved decoupling capabilities," *IEEE Transactions on Power Electronics*, vol. 31, no. 7, pp. 5290-5305, 2016.
- [8] F. Briz and M. Hinkkanen, "Design, implementation and performance of synchronous current regulators for AC drives," *Chinese Journal of Electrical Engineering*, vol. 4, no. 3, pp. 53-65, 2018.
- [9] A. M. Diab *et al.*, "Fast and Simple Tuning Rules of Synchronous Reference Frame Proportional-Integral Current Controller," *IEEE Access*, pp. 1-1, 2021.
- [10] F. Briz, M. W. Degner, and R. D. Lorenz, "Analysis and design of current regulators using complex vectors," *IEEE Transactions on Industry Applications*, vol. 36, no. 3, pp. 817-825, 2000.
- [11] K. Hyunbae and R. D. Lorenz, "A virtual translation technique to improve current regulator for salient-pole AC machines," in *2004 IEEE 35th Annual Power Electronics Specialists Conference (IEEE Cat. No.04CH37551)*, 2004, vol. 1, pp. 487-493 Vol.1.
- [12] S. N. Vukosavic, L. S. Peric, and E. Levi, "Digital Current Controller With Error-Free Feedback Acquisition and Active Resistance," *IEEE Transactions on Industrial Electronics*, vol. 65, no. 3, pp. 1980-1990, 2018.
- [13] S. Li, B. Sarlioglu, S. Jurkovic, N. R. Patel, and P. Savagian, "Analysis of Temperature Effects on Performance of Interior Permanent Magnet Machines for High Variable Temperature Applications," *IEEE Transactions on Industry Applications*, vol. 53, no. 5, pp. 4923-4933, 2017.

## APPENDIX

Coefficients of (17)

$$\begin{aligned}
 t_5 &= \frac{T_d^2 b_o L}{12}, \quad t_4 = \left[ \frac{T_d^2}{12} (b'_o r_s + b'_o L l_1 + K_p) + 0.5 T_d b'_o L \right] + j \omega_r \left[ \frac{T_d^2}{12} b'_o L \right] \\
 t_3 &= \left[ b'_o L + 0.5 T_d (-K_p + b'_o L l_1 + r_s b_o) + \frac{T_d^2}{12} (b'_o r_s l_1 + l_2 + l_1 K_p) \right] + j \omega_r \left[ \frac{b'_o L T_d^2}{12} + 0.5 L T_d b'_o l_1 \right] \\
 t_2 &= \left[ r_s b'_o + b'_o L l_1 + 0.5 T_d r_s b_o l_1 - 0.5 T_d l_2 + K_p - 0.5 K_p T_d l_1 + \frac{T_d^2 l_2 K_p}{12} \right] + j \omega_r [b_o L + 0.5 L T_d b'_o l_1 L] \\
 t_1 &= [b'_o r_s l_1 + l_2 + K_p l_1 - 0.5 l_2 K_p T_d] + j \omega_r [L b'_o l_1], \quad t_0 = K_p l_2, \quad y_2 = \frac{T_d^2}{12} K_p, \quad y_1 = -0.5 K_p T_d, \quad y_0 = K_p
 \end{aligned}$$

Coefficients of (22)

$$\begin{aligned}
 c_5 &= \frac{T_d^2 b_o L}{12}, \quad c_4 = \left[ \frac{T_d^2}{12} (b'_o r_s + b'_o L l_1 + K_p) + 0.5 T_d b'_o L \right] + j \omega_r \left[ \frac{T_d^2}{12} b'_o (L - \hat{L}) \right] \\
 c_3 &= \left[ 0.5 T_d (-K_p + r_s b'_o) + \frac{T_d^2}{12} (b'_o r_s l_1 + l_2 + l_1 K_p) \right] + j \omega_r (L - \hat{L}) \left[ \frac{T_d^2}{12} b'_o l_1 + 0.5 T_d b'_o \right] \\
 c_2 &= \left[ r_s b'_o + b'_o L l_1 + 0.5 T_d l_2 + K_p - 0.5 K_p T_d l_1 + K_p \frac{T_d^2 l_2}{12} \right] + j \omega_r [b'_o (L - \hat{L})], \quad c_1 = [l_2 + K_p l_1 - 0.5 l_2 K_p T_d], \quad c_0 = K_p l_2
 \end{aligned}$$

- [14] A. Diab, M. Rashed, J. Li, C. Gerada, and S. Bozhko, "Performance Analysis of PMSM for High-Speed Starter-Generator System," in *2018 IEEE International Conference on Electrical Systems for Aircraft, Railway, Ship Propulsion and Road Vehicles & International Transportation Electrification Conference (ESARS-ITEC)*, 2018, pp. 1-7.
- [15] M. D. Soricellis, D. D. Rù, and S. Bolognani, "A Robust Current Control Based on Proportional-Integral Observers for Permanent Magnet Synchronous Machines," *IEEE Transactions on Industry Applications*, vol. 54, no. 2, pp. 1437-1447, 2018.
- [16] Y. I. Son, I. H. Kim, D. S. Choi, and H. Shim, "Robust Cascade Control of Electric Motor Drives Using Dual Reduced-Order PI Observer," *IEEE Transactions on Industrial Electronics*, vol. 62, no. 6, pp. 3672-3682, 2015.
- [17] H. Luo, X. Yang, M. Krueger, S. X. Ding, and K. Peng, "A Plug-and-Play Monitoring and Control Architecture for Disturbance Compensation in Rolling Mills," *IEEE/ASME Transactions on Mechatronics*, vol. 23, no. 1, pp. 200-210, 2018.
- [18] J. Han, "From PID to Active Disturbance Rejection Control," *IEEE Transactions on Industrial Electronics*, vol. 56, no. 3, pp. 900-906, 2009.
- [19] H. Sira-Ramírez, J. Linares-Flores, C. García-Rodríguez, and M. A. Contreras-Ordaz, "On the Control of the Permanent Magnet Synchronous Motor: An Active Disturbance Rejection Control Approach," *IEEE Transactions on Control Systems Technology*, vol. 22, no. 5, pp. 2056-2063, 2014.
- [20] B. Du, S. Wu, S. Han, and S. Cui, "Application of Linear Active Disturbance Rejection Controller for Sensorless Control of Internal Permanent-Magnet Synchronous Motor," *IEEE Transactions on Industrial Electronics*, vol. 63, no. 5, pp. 3019-3027, 2016.
- [21] B. Guo, S. Bacha, and M. Alamir, "A review on ADRC based PMSM control designs," in *IECON 2017 - 43rd Annual Conference of the IEEE Industrial Electronics Society*, 2017, pp. 1747-1753.
- [22] G. Herbst, "Practical Active Disturbance Rejection Control: Bumpless Transfer, Rate Limitation, and Incremental Algorithm," *IEEE Transactions on Industrial Electronics*, vol. 63, no. 3, pp. 1754-1762, 2016.
- [23] A. M. Diab, S. Bozhko, M. Galea, and C. Gerada, "Stable and Robust Design of Active Disturbance Rejection Current Controller for Permanent Magnet Machines in Transportation Systems," *IEEE Transactions on Transportation Electrification*, pp. 1-1, 2020.
- [24] J. F. Donoghue, "A Comparison of the Smith Predictor and Optimal Design Approaches for Systems with Delay in the Control," *IEEE Transactions on Industrial Electronics and Control Instrumentation*, vol. IECI-24, no. 1, pp. 109-117, 1977.
- [25] B. K. Kim and Z. Bien, "Design of a Time-Optimal Feedback Controller for Systems with Delay in Control," *IEEE Transactions on Industrial Electronics and Control Instrumentation*, vol. IECI-28, no. 1, pp. 28-36, 1981.
- [26] G. Zhiqiang, "Scaling and bandwidth-parameterization based controller tuning," in *Proceedings of the 2003 American Control Conference*, 2003., 2003, vol. 6, pp. 4989-4996.
- [27] M. F. Golnaraghi, *Automatic control systems*, 9th ed. / Farid Golnaraghi, Benjamin C. Kuo. ed. Hoboken, N.J.: Hoboken, N.J. : Wiley, 2010.
- [28] J. Holtz, Q. Juntao, J. Pontt, J. Rodriguez, P. Newman, and H. Miranda, "Design of fast and robust current regulators for high-power drives based on complex state variables," *IEEE Transactions on Industry Applications*, vol. 40, no. 5, pp. 1388-1397, 2004.
- [29] F. B. d. Blanco, M. W. Degner, and R. D. Lorenz, "Dynamic analysis of current regulators for AC motors using complex vectors," *IEEE Transactions on Industry Applications*, vol. 35, no. 6, pp. 1424-1432, 1999.
- [30] J. Holtz, "The representation of AC machine dynamics by complex signal flow graphs," *IEEE Transactions on Industrial Electronics*, vol. 42, no. 3, pp. 263-271, 1995.
- [31] Y. Liao, F. Li, H. Lin, and J. Zhang, "Discrete current control with improved disturbance rejection for surface-mounted permanent magnet synchronous machine at high speed," *IET Electric Power Applications*, vol. 11, no. 7, pp. 1333-1340, 2017.
- [32] R. Miklosovic, A. Radke, and G. Zhiqiang, "Discrete implementation and generalization of the extended state observer," in *2006 American Control Conference*, 2006, p. 6 pp.
- [33] A. Sayem, Z. Cao, Z. Man, and R. Chuei, "Discrete extended state observer based repetitive control system for improved disturbance rejection performance," in *2016 IEEE 11th Conference on Industrial Electronics and Applications (ICIEA)*, 2016, pp. 743-746.

- [34] R. Desai, B. M. Patre, and S. N. Pawar, "Active disturbance rejection control with adaptive rate limitation for process control application," in *2018 Indian Control Conference (ICC)*, 2018, pp. 131-136.



**Ahmed M. Diab** (S'21) received the B.Sc. (Hons.) and M.Sc. degrees from Zagazig University, Zagazig, Egypt in 2011 and 2016, respectively. He is currently working toward the Ph.D. degree at the University of Nottingham Ningbo China and Institute for Aerospace technology (IAT), university of Nottingham, Nottingham, UK. From 2011 to 2016, he was a research and Teaching Assistant with the Department of Electrical Power and Machines, Zagazig University. His research interests include modeling, control, and stability in high-speed Motor/generator systems for transportation electrification applications and in variable-speed wind generators.



**Seang Shen Yeoh** received the M.Sc. degree in power electronics and drives and the Ph.D. degree in electrical engineering from the University of Nottingham, Nottingham, U.K., in 2011 and 2016, respectively.

Since 2016, he has been a Research Fellow with the Power Electronics, Machines, and Control (PEMC) Research Group, University of Nottingham. His current research interests include modeling and stability studies of complex power systems, and control strategies for power electronic drive systems.



**Serhiy Bozhko** (M'96–SM'18) received the M.Sc. and Ph.D. degrees in electromechanical systems from the National Technical University of Ukraine, Kyiv, Ukraine, in 1987 and 1994, respectively. Since 2000, he has been with the Power Electronics, Machines and Controls Research Group, University of Nottingham, Nottingham, U.K., where he is currently a Professor of Aircraft Electric Power Systems. He is leading several EU- and industry-funded projects in the area of electric power systems for aerospace, including power generation, distribution, and conversion, power quality, control and stability issues, power management and optimization, as well as advanced modeling and simulations methods.



**Chris Gerada** (M'05–SM'12) received the Ph.D. degree in numerical modeling of electrical machines from the University of Nottingham, Nottingham, U.K., in 2005. He subsequently worked as a Researcher with the University of Nottingham on high performance electrical drives and on the design and modeling of electromagnetic actuators for aerospace applications. In 2008, he was appointed as a Lecturer in Electrical Machines; in 2011, as an Associate Professor; and in 2013, as a Professor with the University of Nottingham.

His main research interests include the design and modeling of high-performance electric drives and machines. Dr. Gerada serves as an Associate Editor for the IEEE TRANSACTIONS ON INDUSTRY APPLICATIONS and is the past Chair of the IEEE IES Electrical Machines Committee.



**Michael Galea** (M'13–SM'18) received the Ph.D. degree in electrical machines design from the University of Nottingham, Nottingham, U.K., in 2013. He was appointed as Lecturer in 2014, as an Associate Professor in 2018 and as a Professor in Electrical Machines and Drives in 2019, all with the University of Nottingham. He is currently the Head of the School of Aerospace, University of Nottingham Ningbo China, where he is also the Director of Aerospace. He currently lectures in Electrical Machines and Drives and in Aerospace Systems Integration and manages a number of diverse projects and programs related to the more/all electric aircraft, electrified propulsion, and associated fields. His main research interests include design and development of electrical machines and drives (classical and unconventional), reliability and lifetime degradation of electrical machines, and the more electric aircraft.